THE UNIVERSITY of EDINBURGH

Edinburgh Research Explorer

Influence of Biochar Composition and Source Material on Catalytic Performance: The Carboxylation of Glycerol with CO2 as a Case Study

Citation for published version:
Collett, C, Mašek, O, Razali, N & Mcgregor, J 2020, 'Influence of Biochar Composition and Source Material on Catalytic Performance: The Carboxylation of Glycerol with CO2 as a Case Study', *Catalysts*, vol. 10, no. 9, pp. 1067. https://doi.org/10.3390/catal10091067

Digital Object Identifier (DOI):
10.3390/catal10091067

Link:
Link to publication record in Edinburgh Research Explorer

Document Version:
Publisher's PDF, also known as Version of record

Published In:
Catalysts

Publisher Rights Statement:
© 2020 by the authors. Licensee MDPI, Basel, Switzerland. This article is an open access article distributed under the terms and conditions of the Creative Commons Attribution (CC BY) license (http://creativecommons.org/licenses/by/4.0/).

General rights
Copyright for the publications made accessible via the Edinburgh Research Explorer is retained by the author(s) and / or other copyright owners and it is a condition of accessing these publications that users recognise and abide by the legal requirements associated with these rights.

Take down policy
The University of Edinburgh has made every reasonable effort to ensure that Edinburgh Research Explorer content complies with UK legislation. If you believe that the public display of this file breaches copyright please contact openaccess@ed.ac.uk providing details, and we will remove access to the work immediately and investigate your claim.

Download date: 04. May. 2023

catalysts

MDPI

Article

Influence of Biochar Composition and Source Material on Catalytic Performance: The Carboxylation of Glycerol with CO_2 as a Case Study

Catherine Collett [1], Ondřej Mašek [2], Nurul Razali [1,†] and James McGregor [1,*]

[1] Department of Chemical and Biological Engineering, University of Sheffield, Mappin Street, Sheffield S1 3JD, UK; catherine.collett@nottingham.ac.uk (C.C.); nrazali01@gmail.com (N.R.)
[2] UK Biochar Research Centre, School of Geosciences, University of Edinburgh, Edinburgh EH9 3JN, UK; ondrej.masek@ed.ac.uk
* Correspondence: james.mcgregor@sheffield.ac.uk; Tel.: +44-(0)114-222-4918
† Present address: Faculty of Ocean Engineering Technology and Informatics, Universiti Malaysia Terengganu, 21300 Kuala Terengganu, Terengganu, Malaysia.

Received: 17 August 2020; Accepted: 11 September 2020; Published: 17 September 2020

Abstract: The impact of the chemical and physical composition of biochar catalysts is demonstrated in the carboxylation of glycerol with carbon dioxide for the first time, using acetonitrile as a dehydrating agent. Biochars are an important emerging class of catalytic material that can readily be produced from low-value biomass residues; however, the impact of feedstock choice is often overlooked. The ash content of biochar from three different feedstocks is shown to be catalytically active for the production of glycerol carbonate and triacetin, whilst low-ash catalysts such as soft wood biochar and commercial activated charcoal are inactive. Following treatment with hydrochloric acid, yields of glycerol carbonate over ash were reduced by over 94%, and triacetin was no longer produced. This has been attributed to the loss of potassium content. Carbon content was shown to be catalytically active for the synthesis of diacetin, and graphitic carbon may be beneficial. Through the development of structure–performance relationships, biomass feedstocks with the most suitable properties can therefore be selected to produce biochars for specific catalytic applications. This would expand the range of reactions which can be effectively catalysed by these materials and enhance the development of a more circular and sustainable chemicals industry.

Keywords: heterogeneous catalysis; carbon-based materials; biochar; valorisation; CO_2 utilisation; glycerol carbonate

1. Introduction

The conversion of glycerol to glycerol carbonate using carbon dioxide (CO_2) is a reaction which tackles a number of sustainability issues. The reagents (CO_2 and glycerol) are both waste products; CO_2 emissions contribute to climate change, whilst glycerol is a waste product from biodiesel manufacture. In 2018, 62% of global glycerol production came from biodiesel manufacture [1]. The product, glycerol carbonate, is a precursor to the manufacture of epichlorohydrin and glycidol, which are used in polymer production [2,3]. Further applications of glycerol carbonate are summarised in Figure 1. The reaction therefore offers a sustainable route to valuable products from waste materials.

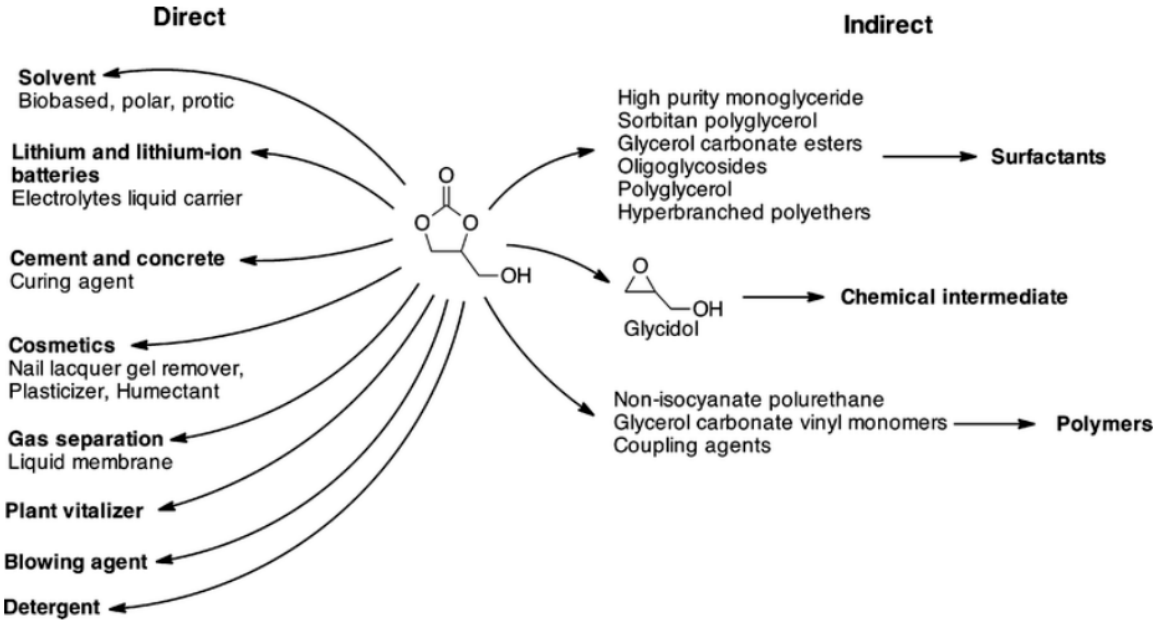

Figure 1. Direct and indirect applications of glycerol carbonate. Figure reproduced with permission from the Royal Society of Chemistry [2].

The synthesis of glycerol carbonate from glycerol is a growing area of research interest. Several reaction pathways to glycerol carbonate have been investigated [2]. In the synthesis of glycerol carbonate from glycerol and CO_2, direct carboxylation of glycerol leads to the formation of water, as shown in Figure 2. The reaction mechanism has been proposed in the literature [4]. The removal of water can favour the production of glycerol carbonate, as the equilibrium is shifted further towards the product side. A review of dehydrating agents can be found in the literature [5–7].

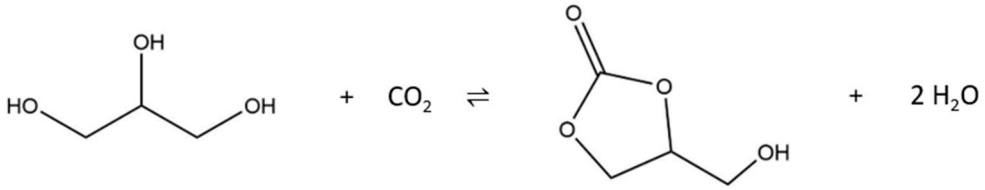

Figure 2. Reaction of glycerol with CO_2 to form glycerol carbonate and water.

Acetonitrile has previously been successfully tested as a dehydrating agent [5,6]. The use of acetonitrile as a dehydrating agent leads to the formation of acetins, as shown in Figure 3. These acetins are valuable products, finding applications as plasticisers, fuel additives and humectants [8]. The acetins formed can be mono-, di- or triacetins, depending on the extent of the reaction. Catalysts are reported in the literature to be necessary for the formation of di- and triacetin [9]. Monoacetin is thought to be produced in the absence of catalyst. The selective production of triacetin is a particular challenge in the literature and is thought to be correlated with Brønsted acidity; steric hindrance may also play a role when microporous catalysts are employed [9,10].

Catalysts used for glycerol upgrading are generally bases, e.g., metal oxides, such as tin and rhodium [2]. The effectiveness of zeolites and lanthanum-based catalysts has also been studied [7,11–13]. However, rhodium is a platinum group metal and is very expensive, whilst tin is moderately scarce, and could be depleted in the next 100–1000 years [13]. Carbonaceous catalysts could therefore improve the economic viability and sustainability of the process through the use of catalytic materials from a renewable resource. Carbonaceous catalysts have largely been employed as support materials, or as feedstocks for the production of sulfonated carbonaceous catalysts; the use of solid acid catalysts for

glycerol acetylation was recently reviewed in the literature [8]. Boiler ash has also been observed to catalyse the reaction, with the activity attributed to potassium silicate [14].

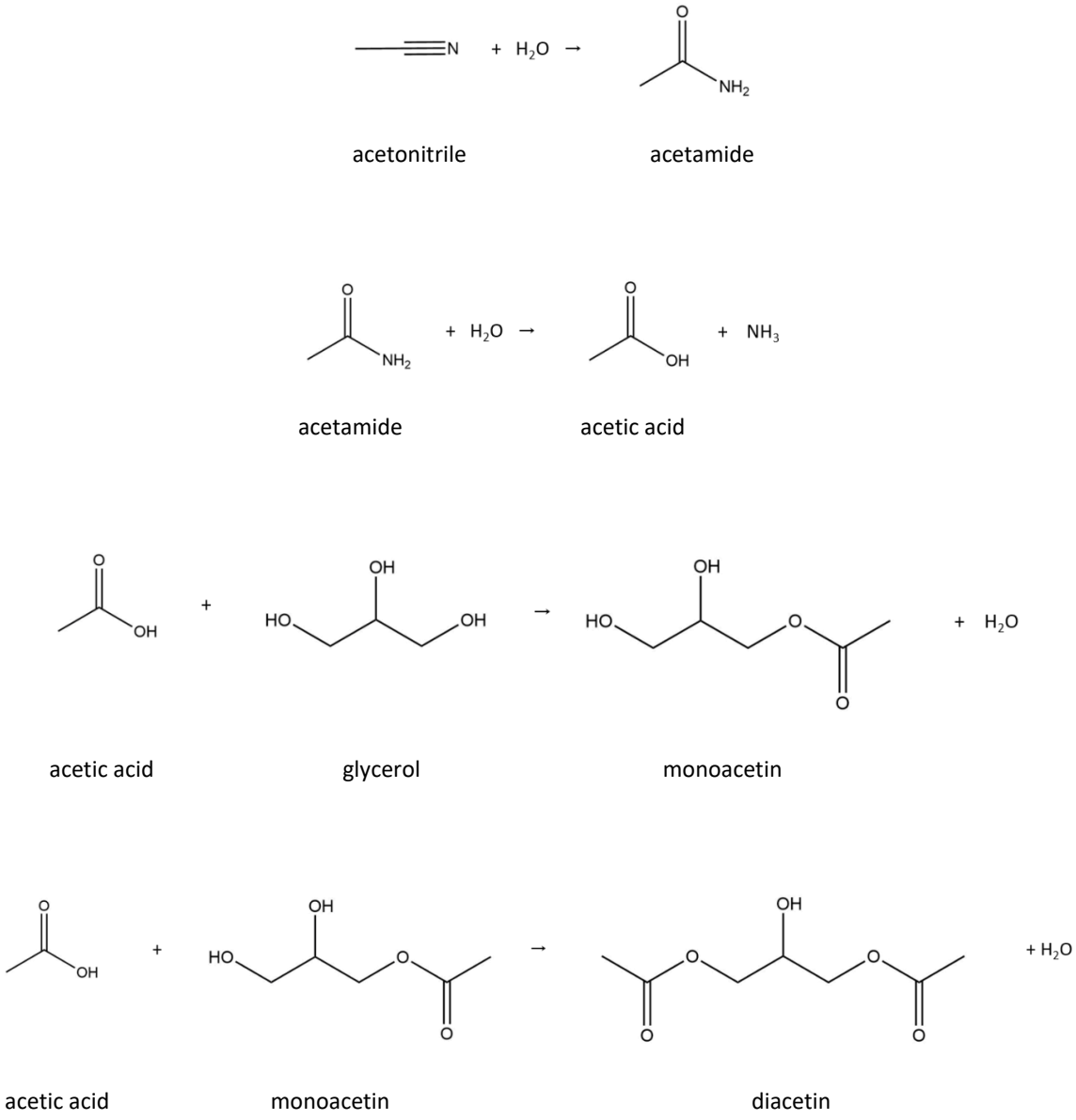

Figure 3. Reactions for the formation of mono-, di- and triacetin from glycerol and acetonitrile.

In the present work, the efficacy of biochars in catalysing this reaction is demonstrated for the first time and the origins of the observed catalytic activity are investigated through a comparison of biochars of differing origin and hence composition. Biochar is a carbonaceous material formed by heating biomass in the absence of oxygen (pyrolysis). The biomass can be sourced from a wide range of feedstocks, such as food, animal and municipal waste, as well as plant materials. The primary application of biochar is in soil remediation to improve crop yields [15,16]. It should be noted that carbonaceous catalysts derived from biomass should not be described as "metal-free" due to the presence of trace metal content in the biomass feedstock. The metal-containing ash can contribute to the catalytic activity of the carbonaceous material; this has been demonstrated in methane decomposition [17].

Biochar has found numerous applications in catalytic research, principally as a support and as a functionalised carbon. This is a fast-growing subject of research interest, with a number of reviews published in recent years [18–21]. The ability to modify the properties of biochar could make this material an excellent candidate for catalytic applications [22]. Properties such as total carbon content

and mineral elements are strongly dependent on feedstock [23], whilst carbon content, ash content, graphiticity, surface area and pH of biochar are dependent on the pyrolysis temperature [23–28]. Notably, ash content can vary from 0 wt.% in wood-based chars to over 50 wt.% in rice-based chars [23,25]. However, studies of the influence of pyrolysis conditions and feedstock on catalytic performance are limited.

There are differing approaches to studying the potential of biochar in catalysis. In many studies, only one feedstock is studied. A representative sample of literature sources is shown in Table 1. In most cases, the rationale for the choice of feedstock is that it is available, and the focus is on optimising the biochar for the application. It is more common for studies of biochars for soil remediation to take an application-centred approach, considering several feedstocks, and recommending the one with the optimal performance [23,25,29–31]. The implicit assumption in many catalytic studies is that the choice of biochar feedstock has limited influence on the subsequent catalytic activity.

Table 1. A sample of literature sources studying biochar for catalytic applications.

Reference	Biochar(s) Studied	Target Application
[32]	Commercial biomass char (type unspecified), pinewood char, pinewood ash	Tar reduction
[33]	Three commercial hardwood chars	Biodiesel production (solid acid catalyst)
[34]	Pelletised peanut hulls, pine pellets, pine chip char	Esterification of fatty acids (solid acid catalyst)
[35]	Pistachio hull biochar	Ozonation of water recalcitrant concentrations
[36]	Pine chip, wood-based activated carbon	Catalyst (solid acid) for hemicellulose hydrolysis
[37]	Karanja seed shells	Esterification of glycerol with acetic acid
[38]	Rice husk char	Conversion of tar using rice husk char-supported nickel–iron catalysts
[39]	Shengli brown coal	Pyrolysis and gasification of biomass
[40]	Woody biomass	(Solid acid) Transesterification of canola oil
[41]	Modified cotton biochar	Low-temperature selective catalytic reduction (SCR) of NO
[42]	Calcium oxide-based catalyst from palm kernel shell biochar	Transesterification of sunflower oil with methanol to produce biodiesel
[43]	Fly ash and eggshell-derived solid catalysts	Solid base catalyst, transesterification of soybean oil to biodiesel
[44]	Ash from cocoa pod husks (supported and unsupported)	Transesterification of soybean oil to biodiesel (Supported and unsupported catalysts)
[45]	Palm bunch ash, support for KOH	Biodiesel synthesis (simultaneous ozonolysis and transesterification)
[46]	Rice husk biochar	Tar reforming
[47]	Miscanthus straw, soft wood	Photocatalytic phenol degradation, oxidation of methanol

In this work, the objective is to explore the potential of biochar catalysts from a range of feedstocks in the synthesis of glycerol carbonate from glycerol and CO_2. This will enable the influence of feedstock and hence biochar composition on catalytic activity to be investigated. Acetonitrile will be used as a dehydrating agent. The use of acetonitrile has not previously been studied using carbonaceous catalysts. The effect of biochar on acetin synthesis will also be studied, with a focus on triacetin production.

2. Results

This work aimed to investigate the origins of catalytic activity of biochar from different feedstocks in glycerol upgrading. The catalytic activity of biochars from different feedstocks is demonstrated in Section 2.1. The results from this initial screening indicated that ash content was the dominant influence on the activity of the catalysts for glycerol carbonate synthesis, but that carbon content catalysed the formation of diacetin. The influence of carbon was studied by comparing two low-ash-content carbons and is presented in Section 2.2. The effect of removing the ash content was tested by comparing the activity of untreated and demineralised biochars, and the ash content was also tested separately for

catalytic activity. These results are shown in Section 2.3. These results confirmed that the ash content from biochar in isolation is catalytically active. The impact of removing potassium from the ash content is demonstrated in Section 2.4.

2.1. Characterisation and Activity of Untreated Biochar: Influence of Ash Content

The reaction was first run without catalyst to confirm which products could be expected in the absence of catalyst. The gas chromatography–mass spectrometry (GC–MS) chromatogram is shown in Figure 4. The reaction leads to a wide range of products, and a full analysis of the products is beyond the scope of the current work. This paper focuses on glycerol carbonate, monoacetin, diacetin and triacetin. As shown in Figure 4, diacetin (retention time 19 min) and triacetin (retention time 17 min) could not be detected in the absence of catalyst. A small peak corresponding to glycerol carbonate was only detected in the first repeat; therefore, glycerol carbonate is not reliably produced in verifiable quantities in the absence of catalyst.

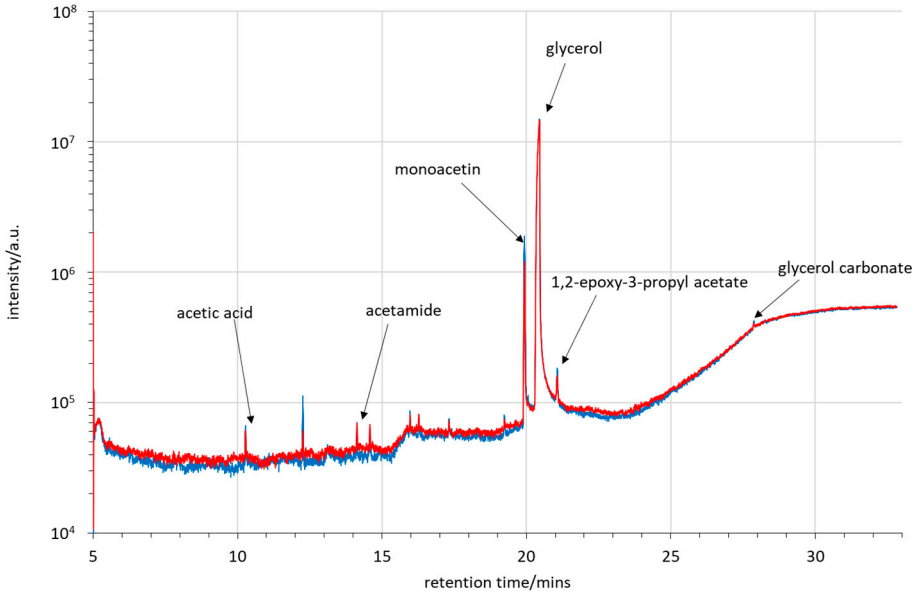

Figure 4. Gas chromatography–mass spectrometry (GC–MS) spectra of reaction products in the absence of catalyst. Two repeats are shown. Note that diacetin (retention time 19 min) and triacetin (retention time 17 min) are not detected. Glycerol carbonate was only detected for one of the two repeats.

The activity of biochar was then compared for four different feedstocks, as well as a commercial activated carbon (AC). In addition, the influence of pyrolysis temperature was compared for oil seed rape where temperatures of 500 °C and 700 °C were employed. The feedstocks were rice husks (RH 550), oil seed rape (OSR 550 and OSR 700), soft wood (SWP 550) and wheat straw (WSP 550). The characterisation data from the biochars are shown in Table 2. Notable differences in their properties included the range of surface areas and the range of ash contents. The surface areas ranged from 51.7 m^2 g^{-1} for WSP 550, to 390 m^2 g^{-1} for SWP 550. The commercial activated carbon had the highest surface area (729 m^2 g^{-1}). The ash content varied from 0% in SWP 550 to 42.9 wt.% in RH 550; this is reflected in the varying surface elemental compositions in Table 2. The only elements detected in SWP 550 were C and O.

Table 2. Summary of the characterisation of biochars from different feedstocks (rice husk (RH), oil seed rape (OSR), wheat straw (WSP) and soft wood (SWP)) and compared with a commercial activated carbon (AC). A dash indicates that experimental data is not available. Results for elemental composition reported to one decimal place.

Property	RH 550	OSR 550	OSR 700	WSP 550	SWP 550	AC
Structure						
BET area/m^2 g^{-1}	121	62.3	107	51.7	390	729
Micropore volume/cm^3 g^{-1}	3.25×10^{-3}	0.0	1.88×10^{-2}	2.86×10^{-3}	1.05×10^{-1}	1.54×10^{-1}
Median Pore Width/Å	7.671	11.143	7.739	8.854	7.663	7.657
Proximate Composition						
Moisture/wt.%	2.98	4.25	1.49	1.01	3.52	6.88
Volatile/wt.%	9.39	14.40	10.40	12.70	16.70	4.13
Fixed carbon/wt.%	44.50	67.40	67.80	67.30	81.70	84.70
Ash/wt.%	42.90	13.60	20.30	18.90	0.00	4.25
Surface Elemental Composition						
C/at.%	67.6	67.8	65.9	69.2	90.4	-
O/at.%	20.3	12.5	21.9	20.4	9.6	-
Si/at.%	8.3	1.1	2.8	4.5	0.0	-
K/at.%	0.8	17.1	5.9	3.1	0.0	-
Ca/at.%	0.3	0.0	1.1	1.0	0.0	-
Mg/at.%	0.0	0.0	0.4	0.0	0.0	-
Other/at.%	2.8	1.5	2.0	1.9	0.0	-

Fourier transform-infrared spectroscopy (FTIR) spectra of the biochars are shown in Figure 5. The spectra demonstrate that the biochars exhibited broadly similar surface chemistry. The biochars exhibited a C-C band at ~2000 cm^{-1}, aromatic C=C bands at ~1560 cm^{-1}, a weak phenolic O-H band at ~1350 cm^{-1}, and various Si–O attributed to ash content at ~1000 cm^{-1}. The silica bands were not observed in AC or SWP 550, and aromatic C=C bands were not observed strongly in AC or OSR 700. The two peaks between 2300–2400 cm^{-1} are attributed to CO_2. Atmospheric CO_2 is expected to have been subtracted by the background scan. Therefore, the CO_2 peak may be due to CO_2 adsorbed on the surface of the biochars, or due to variations in CO_2 concentration in the atmosphere.

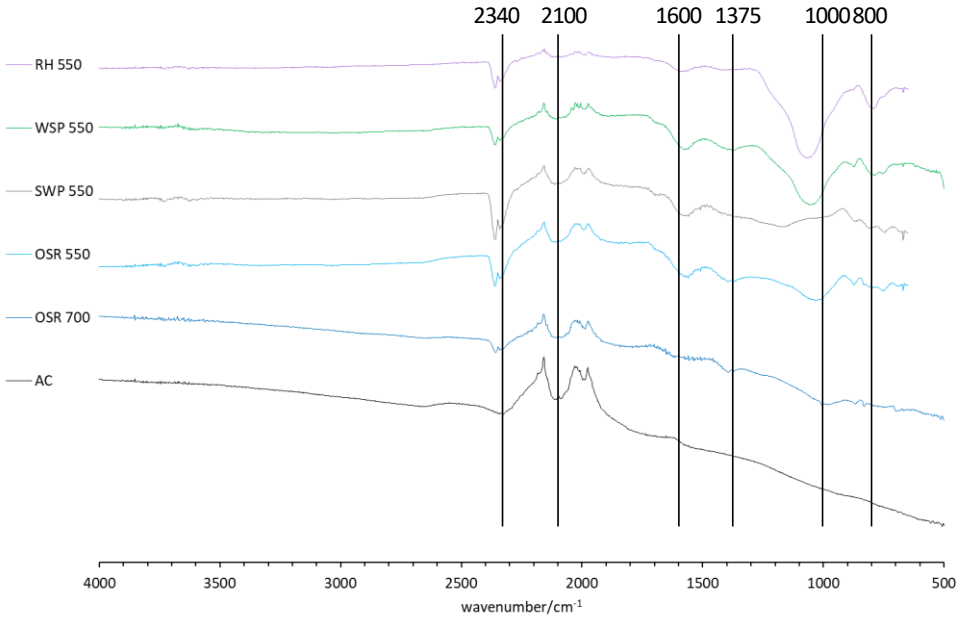

Figure 5. Fourier-transform infrared spectroscopy–attenuated total reflection (FTIR–ATR) spectra for biochars from different feedstocks (rice husk (RH), wheat straw (WSP), soft wood (SWP) and oil seed rape (OSR)) compared with commercial activated carbon (AC). The peaks are attributed to: CO_2 (2340 cm^{-1}), C≡C (2100 cm^{-1}), aromatic C=C (1600 cm^{-1}), phenolic O-H (1375 cm^{-1}), Si-O-Si symmetric (1000 cm^{-1}) and Si-O-Si asymmetric (800 cm^{-1}). Spectra are offset for clarity.

The concentrations of glycerol carbonate, monoacetin, diacetin and triacetin were calibrated, and the results are shown in Figure 6. These results demonstrate that biochars sourced from RH, OSR and WSP are catalytically active for the production of glycerol carbonate, diacetin and triacetin. These products are not detected in the absence of catalyst. Higher yields of monoacetin are also obtained for RH 550 (0.128 mol L^{-1}) and OSR 550 (0.116 mol L^{-1}) compared to the absence of catalyst (0.016 mol L^{-1}). It is notable that glycerol carbonate was not detected when using AC or SWP biochar as catalysts.

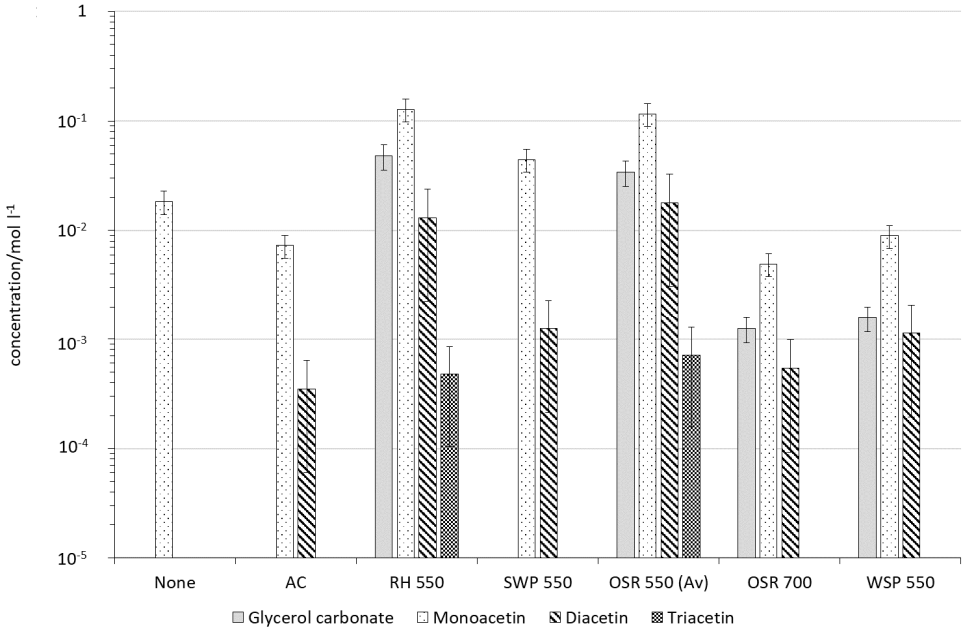

Figure 6. Concentration of liquid phase products (glycerol carbonate, monaocetin, diacetin and triacetin) for carbonaceous materials from four different biochar feedstocks (rice husk (RH), soft wood (SWP), oil seed rape (OSR) and wheat straw (WSP)). These are compared with a commercial activated charcoal (AC) and no catalyst. Error bars are percentage error, estimated from three repeats of OSR 550 (average denoted by (Av)). A logarithmic *y*-axis is used to present high and low concentration products.

The composition and structural properties of the biochars are compared in Table 2. The experimental results indicated that the catalysts with the highest ash contents (RH, OSR and WSP biochars, as shown in Table 2) are the most catalytically active for the synthesis of glycerol carbonate. For instance, RH 550 contains 42.9% ash by mass and yields the greatest quantities of glycerol carbonate and monoacetin. Surface functional groups as observed in Figure 5 did not appear to correlate with catalytic activity; for example, SWP 550, OSR 550 and WSP 550 produced similar FTIR spectra and very different experimental results. Therefore, FTIR spectra are not considered further; additional spectra for ash and demineralised samples are provided in the Supplementary Materials (Figures S2–S4). Biochars with lower or negligible ash content (AC, SWP) were not active for the production of glycerol carbonate. Notably, AC and SWP did lead to the formation of diacetin; these data are analysed further in Section 2.2.

The ash derived from different biochars was therefore tested for its catalytic activity. As shown in Figure 7, the biochar ash from a range of samples was also active for the synthesis of glycerol carbonate, diacetin and triacetin. The concentrations were very comparable to the activity of the untreated biochar. In the case of OSR 550, OSR 700 and WSP 550, the ash yields a greater quantity of products than the untreated biochar. This is also despite the much lower surface areas for the ash content, compared to the biochar (shown in Figure 8). This indicates that the ash content contributes to the activity of the biochar. However, ash is not exclusively responsible for catalytic activity, as the synthesis of diacetin is

observed over materials with no or low ash content (AC and SWP) but is not observed in the absence of a catalyst.

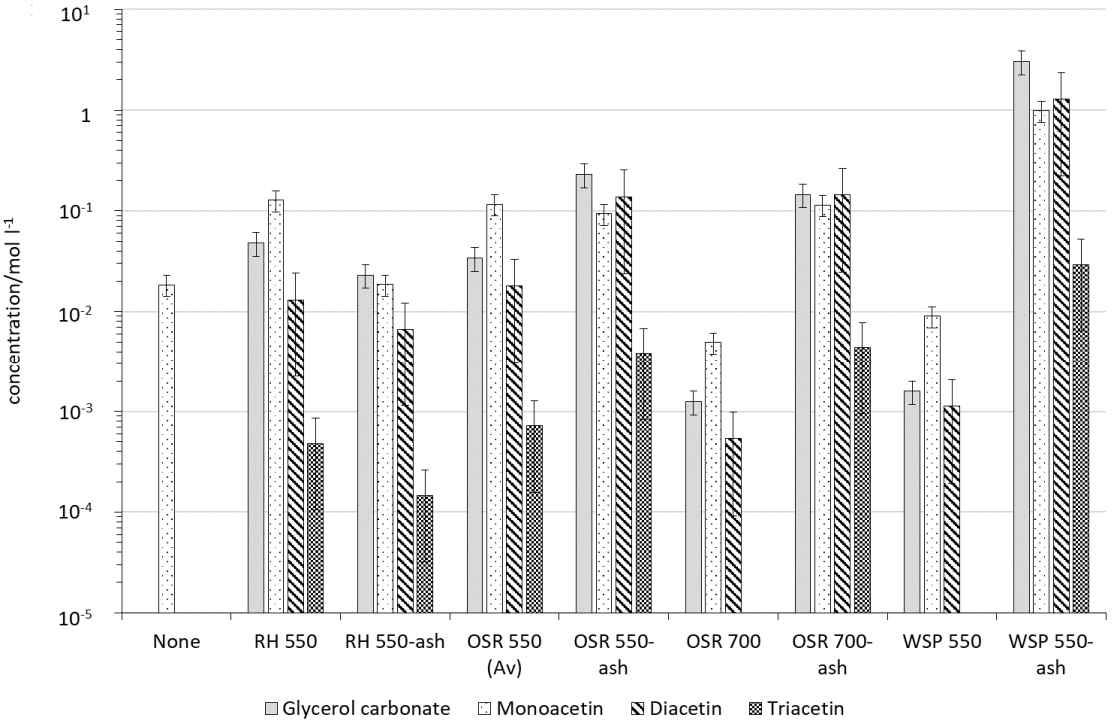

Figure 7. Comparison of production of glycerol carbonate and acetins from biochar and biochar ash from different feedstocks (rice husk (RH), oil seed rape (OSR) and wheat straw (WSP)). (Av) indicates an average of three readings; this was used to estimate the percentage error. A logarithmic *y*-axis is used to present high and low concentration products.

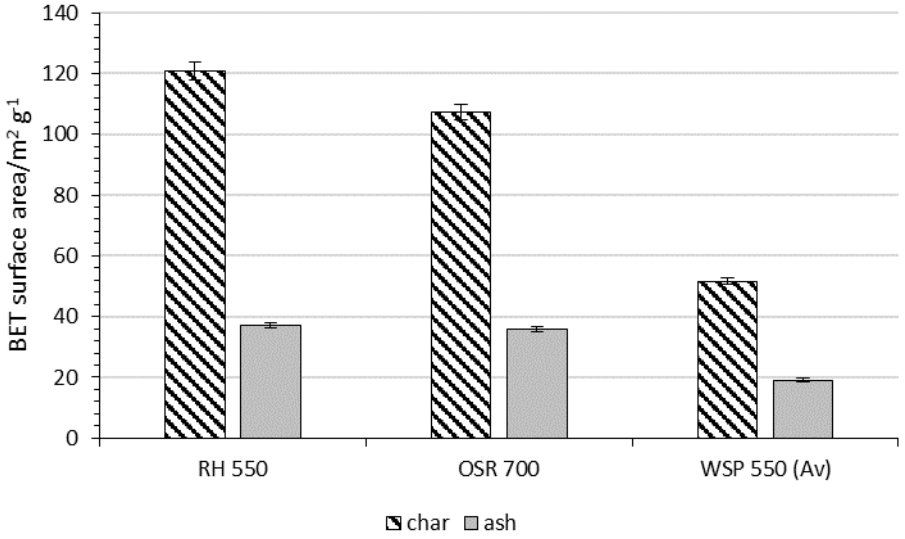

Figure 8. Comparison of BET surface area of biochar and ash from different feedstocks (rice husk (RH), oil seed rape (OSR) and wheat straw (WSP)). Isotherm obtained using N_2 at 77 K. Error bars calculated from three repeats of WSP 550 (denoted by (Av)); standard deviation ± 1.25 m^2 g^{-1}, percentage error 2.42%.

The performance of two biochars from the same feedstock (OSR) were also compared. These were produced at two different pyrolysis temperatures: 550 °C (OSR 550) and 700 °C (OSR 700). As shown

in Figure 9, the catalytic activity of the biochar ashes were highly comparable, leading to similar quantities of glycerol carbonate, monoacetin, diacetin and triacetin. However, OSR 700 demonstrated lower levels of catalytic activity compared to OSR 550, despite having a higher ash content (from Table 2, 20.3% ash for OSR 700 compared to 13.6% ash for OSR 550). Whilst the ash content clearly contributes to catalytic activity, Figure 9 confirms that it is not the only factor, with carbon structure having an influence. The influence of carbon content and ash will be considered in turn.

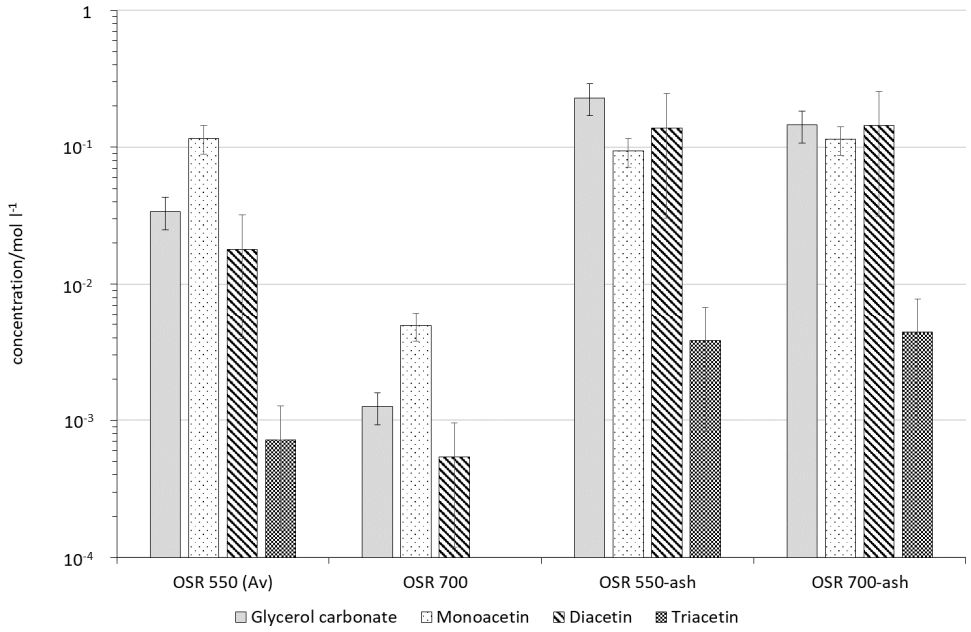

Figure 9. Concentration of glycerol carbonate and acetins produced using oil seed rape (OSR) biochars produced at different pyrolysis temperatures, and their ashes. A logarithmic *y*-axis is used to present high and low concentration products.

These results demonstrate that carbon content and ash content are catalytically active for different aspects of the reaction.

2.2. Role of Carbon

To study the influence of carbon, the biochars with the lowest ash contents were compared: SWP 550 (0 wt.%) and AC (4.25 wt.%). These biochars did not lead to the synthesis of glycerol carbonate or triacetin, but notably, they did catalyse the formation of diacetin, as shown in Figure 6—diacetin was not detected in the absence of a catalyst.

The use of SWP 550 led to higher quantities of monoacetin and diacetin, compared to AC (approximately 6 times higher for monoacetin and 3.5 times higher for diacetin). This is despite SWP 550 having only half the surface area of AC (390 m^2 g^{-1} and 729 m^2 g^{-1}, respectively).

The properties of SWP 550 and AC can be compared using the data in Table 2. For SWP 550, no surface potassium was detected—the only elements detected were carbon and oxygen. AC is also expected to consist primarily of C and O, with some silica in the ash content. However, the carbon structure of these samples does vary, as evidenced by Raman spectroscopy studies. From Raman spectra (Supplementary Materials Figure S1), SWP 550 has a much lower A_{D1}/A_G ratio than AC (1.32 and 2.82, respectively). This indicates that SWP 550 is more graphitic in structure than AC, which could contribute to its catalytic activity.

2.3. Influence of Ash Content on Catalytic Activity of Biochar

The influence of ash content was studied by reducing the ash content of the biochars through demineralisation. As shown by proximate analysis (Table 3), the ash content was not completely removed by this method but was reduced compared to the untreated biochars. Ash removal was most effective in OSR 700, with a reduction in ash content from 20.3% to 14.2%. Demineralisation had the least effect in RH 550, with only a small proportion of ash removed (from 42.9% to 40.1%).

Table 3. Summary of the characterisation of demineralised (denoted by -DM) biochars from different feedstocks (rice husk (RH), oil seed rape (OSR) and wheat straw (WSP)). Shaded cells indicate that experimental data is not available. Results for elemental composition reported to one decimal place.

Property	RH 550-DM	OSR 700-DM	WSP 550-DM
Structure			
BET area/m^2 g^{-1}	86.6	78.8	94.7
Micropore volume/cm^3 g^{-1}	1.83×10^{-3}	9.08×10^{-4}	3.55×10^{-3}
Median Pore Width/Å	7.672	7.688	7.663
Proximate Composition			
Moisture/wt.%	0.60	1.54	0.98
Volatile/wt.%	10.89	10.78	14.90
Fixed carbon/wt.%	48.38	73.48	70.36
Ash/wt.%	40.13	14.20	13.76
Surface Elemental Composition			
C/at.%	70.7	78.7	69.8
O/at.%	20.0	15.3	20.1
Si/at.%	6.2	4.0	8.2
K/at.%	0.0	0.0	0.0
Ca/at.%	0.1	0.4	0.0
Mg/at.%	0.0	0.0	0.0
Other/at.%	3.1	1.6	1.9

The effect of demineralisation on elemental composition was studied through X-ray photoelectron spectroscopy (XPS). Silica content was not removed; however, potassium could no longer be detected on the surface of the samples by XPS (Table 3). There was no reduction in the quantity of any other elements at the surface following demineralisation; therefore, this work focuses on the influence of potassium removal.

The impact of demineralisation on catalyst activity towards glycerol carbonate synthesis varied. As shown in Figure 10, the concentration of glycerol carbonate decreased following demineralisation for RH 550 but increased for OSR 550. Notably, triacetin was not produced following demineralisation for RH 550. The demineralisation appeared to have differing impacts on catalytic activity of different biochars. The impact of demineralisation on the catalytic activity of the ash content was therefore considered separately.

2.4. Characterisation and Activity of Treated Biochar Ash

Biochar ash from untreated and demineralised samples were tested for catalytic activity. The characterisation data is shown in Table 4. BET surface areas were much lower compared to the biochar samples; for the ash samples, the highest surface area was for RH 550-ash at 37.2 m^2 g^{-1}, whereas the lowest surface area in a biochar sample was for WSP 550 at 51.7 m^2 g^{-1} (Table 2). In all cases, surface potassium content was reduced by over 75% following demineralisation. However, trace amounts of potassium (<5 at.%) were still detected at the surface of the demineralised ash samples.

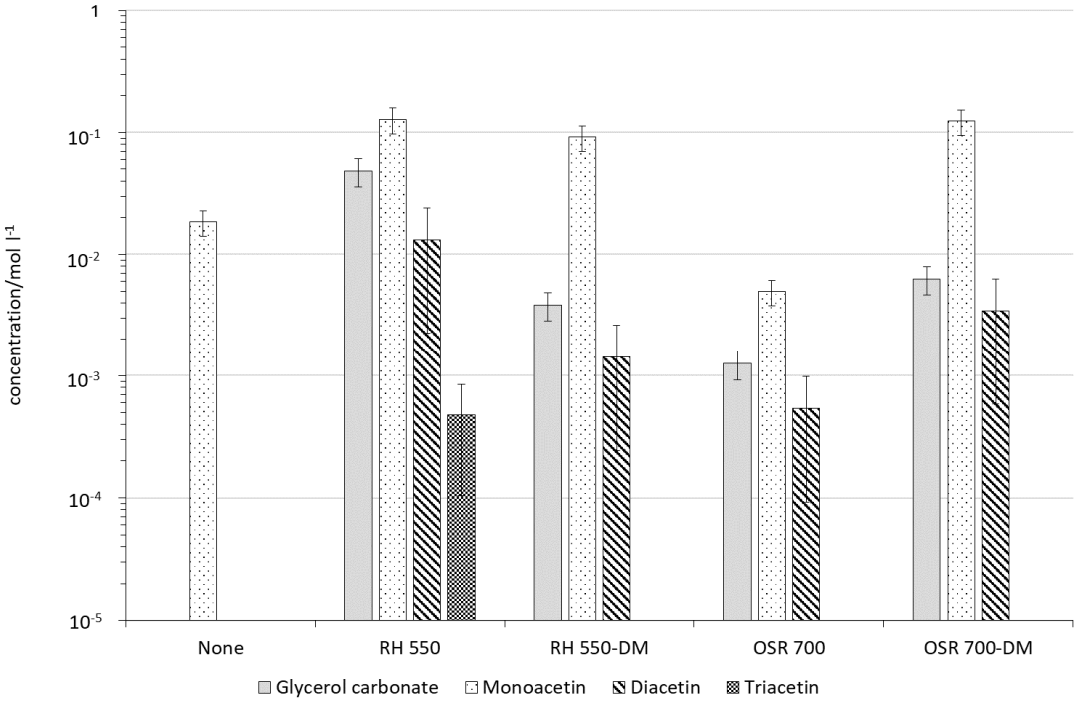

Figure 10. Comparison of production of glycerol carbonate and acetins over biochar from different feedstocks (rice husk (RH) and oil seed rape (OSR)) before and after demineralization (denoted by –DM). A logarithmic *y*-axis is used to present high and low concentration products.

Table 4. Summary of the characterisation of ash samples from untreated and demineralised (denoted by –DM) biochars from different feedstocks (rice husk (RH), oil seed rape (OSR) and wheat straw (WSP)). A dash indicates that experimental data are not available. OSR 550-ash was not characterised—the properties are assumed to be comparable to OSR 700-ash. Results for elemental composition reported to one decimal place.

Property	RH 550-ash	OSR 700-ash	WSP 550-ash	RH 550-DM-ash	OSR 700-DM-ash	WSP 550-DM-ash
Structure						
BET area/m^2 g^{-1}	37.2	35.9	19.1	-	-	-
Micropore volume/cm^3 g^{-1}	1.42×10^{-3}	9.80×10^{-4}	5.67×10^{-4}	-	-	-
Median pore width/Å	10.960	10.985	10.911	-	-	-
Surface Elemental Composition						
C/at.%	5.0	2.0	4.4	3.6	2.2	2.5
O/at.%	59.4	63.4	62.8	68.1	64.9	65.9
Si/at.%	29.5	19.3	22.5	26.5	21.7	27.3
K/at.%	3.5	9.2	6.3	0.6	1.9	0.7
Ca/at.%	0.7	3.3	2.2	0.4	4.7	2.3
Mg/at.%	0.9	1.4	0.6	0.2	2.7	1.0
Other/at.%	1.0	1.4	1.2	0.6	2.0	0.3

The results from reactions using biochar ash as catalysts are shown in Figure 11. Notably, no triacetin was produced using any of the demineralised ash samples, and glycerol carbonate yield was greatly reduced in all cases. RH 550-DM-ash did not lead to the formation of any glycerol carbonate, and yields were reduced by over 94% in OSR 700-ash (OSR 700-ash 0.145 mol L^{-1}; OSR 700-DM-ash 7.64×10^{-3} mol L^{-1}) and by 99.8% in WSP 550-ash (WSP 550-ash 3.05 mol L^{-1}, WSP 550-DM-ash 7.44×10^{-3} mol L^{-1}). This indicates that potassium content influences the production of glycerol carbonate and triacetin.

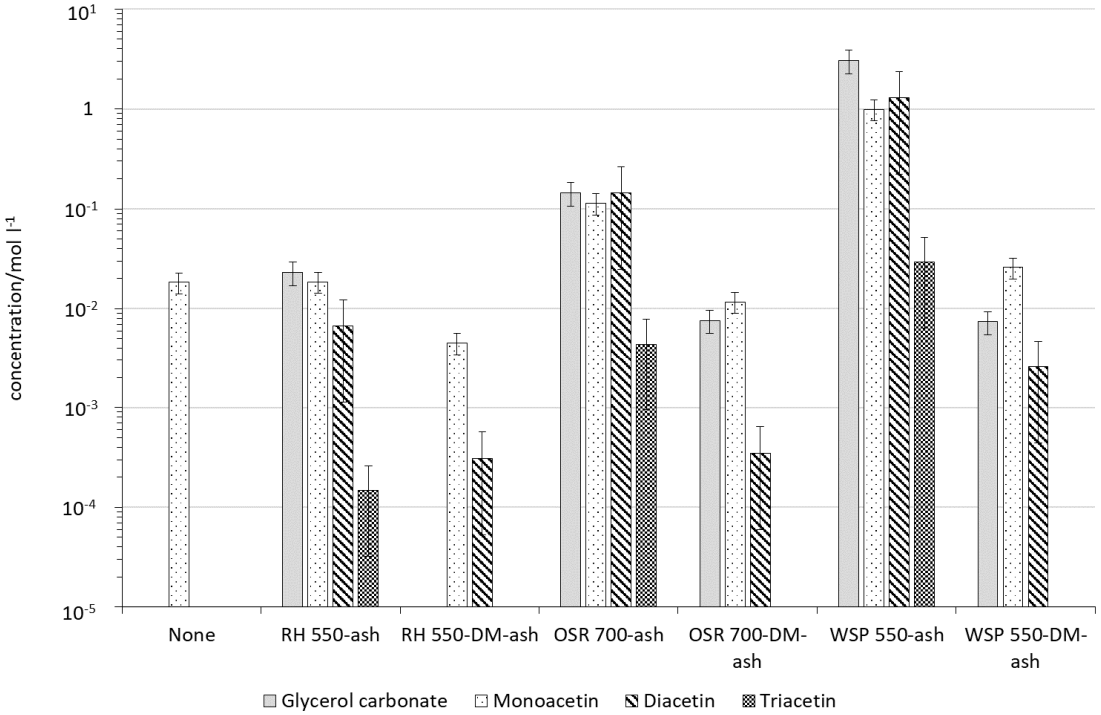

Figure 11. Activity of biochar ash from different feedstocks (rice husk (RH), oil seed rape (OSR) and wheat straw (WSP)) before and after demineralisation; -DM indicates demineralised samples. A logarithmic *y*-axis is used to present high and low concentration products.

3. Discussion

In a number of studies, the influence of different biochar feedstocks on catalytic activity of resulting biochar is not considered, with the main objective of treatments being to activate (or increase the surface area of) the biochar. In the present study, results have shown almost no correlation of activity in untreated biochars with surface area. The highest surface areas are for AC and SWP 550 (729 m^2 g^{-1} and 390 m^2 g^{-1}, respectively); however, these samples produce no glycerol carbonate or triacetin. Similarly, OSR 700 and WSP 550 produce similar quantities of glycerol carbonate, despite OSR 700 having twice the surface area of WSP 550 (107 m^2 g^{-1} vs. 51.7 m^2 g^{-1}, respectively). It should not be assumed that biochars from different feedstocks are comparable or interchangeable, or that treatments are only needed to "activate" or increase surface area. Despite all being "carbonaceous" materials, surface area is clearly not the dominant influence.

Similarly, microporosity and pore size do not appear to have a strong influence on catalyst activity. The median pore width of RH 550 (7.671 Å) is comparable to SWP 550 (7.663 Å) and AC (7.657 Å). However, RH 550 was one of the most active biochars for glycerol carbonate synthesis, and AC and SWP 550 were not effective in this reaction. Porosity is likely to impact activity and has been suggested as impacting selectivity to triacetin in the literature [10]. However, in this case, it does not appear to be the most influential factor.

A much stronger impact is seen for the influence of ash content. This is clear from the data shown in Section 2.1; biochars with negligible ash content (SWP 550 and AC) are inactive for the synthesis of glycerol carbonate and triacetin. In addition, biochar ash is shown to be catalytically active (Figure 7). This is consistent with literature findings that have demonstrated the activity of biochar ash in similar reactions [48,49]. Biochars with higher ash contents, such as RH 550 (42.9 wt.%), are the most active for glycerol carbonate and triacetin synthesis. However, it is not a simple correlation, as the biochar with the lowest ash content (OSR 550 at 13.6 wt.%) produces the highest quantity of triacetin. Therefore, the composition of the ash, as well as the quantity, is clearly influential.

The influence of potassium content is clearly demonstrated in Figure 11, comparing biochar ash from untreated and demineralised samples. In all cases, demineralised biochar ash contains at least 75% less potassium, and glycerol carbonate yields are decreased by over 94%. Triacetin is also not produced in the demineralised samples. The role of potassium on reaction mechanisms is beyond the scope of the current work, but it has been speculated upon in the literature for this reaction and other pathways from glycerol to glycerol carbonate [48,50–53]. From the data shown in this work, potassium content clearly influences the production of glycerol carbonate and triacetin, and it would be worthy of further study. The importance of potassium is further emphasized by its other positive impacts on biochar production and applications for carbon storage [54] and nutrient cycling [55].

Whilst ash and potassium have been shown to have strong influences on the production of glycerol carbonate and triacetin, low-ash samples were also shown to be catalytically active for the synthesis of diacetin. No diacetin was detected in the absence of catalyst, but was produced by both SWP 550 and AC, despite negligible ash content (<5 wt.%). SWP 550 also appears to be catalytically active for the synthesis of monoacetin, with higher quantities produced compared to the absence of catalyst (0.044 mol L^{-1} and 0.015 mol L^{-1}, respectively).

For the synthesis of diacetin, SWP 550 was more active than AC (1.25×10^{-3} mol L^{-1} and 3.5×10^{-4} mol L^{-1}, respectively). This is despite having a lower surface area (390 m^2 g^{-1} and 729 m^2 g^{-1}, respectively), comparable elemental composition (81.7% fixed carbon for SWP 550, 84.7% fixed carbon for AC) and comparable micropore volumes (0.0105 cm^3 g^{-1} and 0.0154 cm^3 g^{-1}, respectively). As SWP 550 only consists of the elements C and O, and AC is assumed to be similar, it appears that the carbon structure exert a strong influence on catalytic activity for diacetin synthesis.

As the focus of this work was the production of glycerol carbonate, the carbon structures of SWP 550 and AC have not been studied in detail, as they did not produce the desired product. Nevertheless, Raman spectroscopy indicates that SWP 550 is more graphitic in structure than AC (A_{D1}/A_G ratios of 1.32 and 2.82, respectively). Several studies in the literature have pointed to the catalytic role of carbon, particularly graphitic carbon [56]. This suggests that the role of graphitic carbon is an area for further study.

A key finding from the current work is that the type of feedstock has a critical influence on catalytic activity. Even before post-synthesis treatment, biochars from four different feedstocks exhibited varying conversion rates and selectivities to a range of products in this reaction (Figure 6). In Table 1, it was highlighted that many studies often consider only one feedstock. This may only provide limited understanding of how best to realise the potential of biochar as a catalyst in this reaction. The development of structure–performance relationships, i.e., identifying which components and physical structures within the biochars give rise to particular catalytic activities, will allow for a more judicious selection of biomass feedstock from which to prepare a suitable biochar catalyst. This will require screening studies using multiple feedstocks, and comprehensive characterisation of the composition of biochar. The successful development of biochar-based catalysts has significant potential sustainability benefits. At end-of-life, biochar catalysts need not be disposed of and instead can be employed for additional purposes, e.g., in agricultural applications to amend soil and sequester carbon. Such ecological environmental benefits stand in contrast to typical metal-based catalysts; upstream mining extraction of the active metal component can have stark negative ecological impacts.

4. Materials and Methods

4.1. Materials

Biochar was sourced from the standard biochar set (www.biochar.ac.uk/standardbiochar) developed by the UK Biochar Research Centre at the University of Edinburgh. The feedstocks chosen were rice husk biochar, wheat straw biochar, oil seed rape biochar and soft wood biochar, which were known to exhibit varying compositions and surface areas, following characterisation by the University of Edinburgh [57]. The biochars used are summarised in Table 5. The biochar was produced in a standardised and

reproducible process in a Stage III unit as described in the literature [58]. The properties of the biochars were compared with a commercial activated charcoal (activated charcoal Norit®, from peat, steam-activated and acid-washed, supplied by Sigma-Aldrich, Gillingham, Dorset, UK).

Table 5. Standard biochars from UK Biochar Research Centre used in this study.

Feedstock	Pyrolysis Temperature(s)/°C	Abbreviation
Rice husk	550	RH 550
Wheat straw pellets	550	WSP 550
Oil seed rape	550 and 700	OSR 550, OSR 700
Soft wood	550	SWP 550

4.2. Sample Preparation

The biochar was supplied in the form of pellets by the UK Biochar Research Centre, which were ground and sieved to under 90 μm in diameter. These biochars were tested for catalytic activity without pre-treatment, activation or metal loading (untreated biochars). Biochar ash samples were prepared through the combustion of biochar in a box furnace at 900 °C for 30 min, resulting in the formation of an amorphous silica-based ash.

The protocol for demineralisation using HCl was developed based on methods in the literature [59–62]. 200 mL of a 3 M solution (Sigma-Aldrich, Gillingham, Dorset, UK) were added to 40 g of crushed and sieved biochar (0.5–1.0 mm), and the mixture was heated and stirred for approximately 36 h at 60 °C. The solution was filtered and rinsed with deionised water and dried overnight in an oven at 105 °C. The sample was washed further in approximately 500 mL of hot deionised water (80 °C) for 2 h, and then was filtered and rinsed with deionised water. The washing water was tested for Cl^- ions by adding a few drops of 0.1 M silver nitrate solution (Sigma-Aldrich, Gillingham, Dorset, UK); a white precipitate indicated the presence of Cl^- ions. Rinsing continued until Cl^- ions were no longer detected. The samples were then dried in an oven at 105 °C overnight.

4.3. Characterisation Methods

FTIR spectra were obtained using a Shimadzu IRAffinity-1S FTIR spectrometer (Shimadzu, Kyoto, Japan) with a Specac Quest ATR diamond puck accessory (Specac, Orpington, Kent, UK) with a 1.8 mm diameter diamond crystal capable of obtaining spectra in the range of 7800 to 400 cm^{-1} [63]. The penetration depth is estimated to be 2.01 μm at 1000 cm^{-1}. In this work, spectra were obtained in the range 400 to 4000 cm^{-1}, with a resolution of 2 cm^{-1}. An atmospheric background (one scan) was used for powdered biochar studies, and the powder was used undiluted. For the Specac Quest ATR, no further sample preparation was required. The samples were scanned 16 times using the Happ–Genzel apodization method in transmittance mode. The spectrum obtained was an average of these 16 scans. After use, the crystal and anvil were cleaned with a cotton bud dipped in distilled water, followed by ethanol, and allowed to dry. A sample scan was performed to check that the surface was dry before loading the next sample.

Thermal gravimetric analysis (TGA) proximate analysis was carried out using a Perkin Elmer TGA (model 4000) (Perkin Elmer, Waltham, Massachusetts, United States). The analysis methods used were based on industrial standards for biochar analysis [64].

Elemental composition was determined by an elemental scan using XPS. The XPS instrument used was a Kratos Ultra instrument (Kratos, Manchester, UK) with a monochromated aluminium source, calibrated using software available from NPL [65]. Two areas were analysed for each sample to account for heterogeneity. Analysis was performed using CasaXPS software (available from casaxps.com).

BET analysis was carried out using a Micromeritics 3Flex Surface Characterisation Analyser (Micromeritics, Norcross, GA, USA). Approximately 0.2 g of sample were prepared for BET and porosimetry analysis. The samples were degassed in a vacuum oven at 120 °C for at least 48 h at a vacuum pressure of 0.1 mbar. They were further degassed at 250 °C for at least 24 h using a Micromeritics

VacPrep 061 Degasser (Micromeritics, Norcross, GA, USA), at a vacuum pressure of approximately 0.02 mbar. The surface area was calculated using the BET equation from N_2 isotherms (>99% purity, BOC) measured at 77 K. Due to difficulties obtaining BET isotherms for OSR 700, an additional heating mantle was used to raise the temperature of the OSR 700 sample tube to 250 °C during the vacuum evacuation stage. Micropore volume was calculated from the adsorption isotherms using Harkins–Jura *t*-plot [66], and median pore width by the Horvath–Kawazoe method [67–71].

Raman spectra were collected using a Renishaw inVia Raman microscope (Renishaw, Wotton-under-Edge, Gloucestershire, UK). A green laser of wavelength 514 nm was used with a source energy of 20 mW at an intensity of 1%. The microscope magnification used was 50×. Three areas were analysed for each sample. Details of the curve deconvolution process are given in the Supplementary Materials, based on methods available in the literature (Table S2) [68–71].

4.4. Reaction Methods

Reactions were performed in a 45 mL autoclave, supplied by Parr Instruments Model 4714 (Parr Instruments, Moline, IL, USA). A silicone oil bath (silicone oil from Alfa Aesar) was used for heating the reactor. The reaction was carried out on an IKA C-MAG HS 7 Magnetic Stirring plate. 0.23 g of biochar was added to 4.6 g of glycerol (>99.0% purity, Sigma-Aldrich) with 5 mL of acetonitrile (>99.5% purity, Sigma-Aldrich) used a dehydrating agent.

A standardised CO_2 loading procedure was used to ensure the same quantity of CO_2 was loaded for all reactions. Prior to reaction, the reactors were loaded for 10 s with CO_2 (BOC, purity > 99.8%) to a pressure of 18 bar, and then depressurised. This was repeated twice more, before loading to 18 bar for 30 s. This resulted in an approximate reaction pressure of 30 bar. The reactor was placed in the silicone oil bath and heated to 160 °C. The reaction time was 22 h, with a stirring rate of approximately 500 rpm.

Due to the high viscosity of glycerol (approximately 1.41 Pa s), the sample was diluted with 10 mL of ethanol of >99% purity (Fisher Scientific, Loughborough, Leicestershire, UK) in the reactor, to allow the contents to be extracted more easily and filtered. Syringe filtration was used to ensure separation of the finest biochar particles from the liquid phase products (Captiva Premium Syringe Layered Filter, glass microfiber pre-filter, nylon membrane, 15 mm diameter, 0.2 μm pore size).

The sample was diluted further for GCMS analysis. 100 μL of filtrate was added to 1 mL of ethanol. The liquid products were analysed using a Shimadzu GC-MS 2010 GCMS (Shimadzu, Kyoto, Japan) fitted with an HP-INNOWAX capillary column (length 30 m, internal diameter 0.25 mm, film thickness 0.25 μm). Helium was used as the carrier gas, with a linear flow rate of 30 cm s^{-1}. The stream split ratio was set at 100. The injector temperature was set at 250 °C. 0.5 μL of sample were injected into the column. The GC–MS analysis method is detailed in Table 6. Calibration samples were prepared for glycerol, glycerol carbonate, mono-, di- and triacetin; further details are given in the Supplementary Materials (Tables S3 and S4, Figures S5–S9).

Table 6. Method used for analysis of products of glycerol upgrading reaction in the GCMS.

Temperature/°C	Hold Time/min	Ramp Rate/°C min^{-1}
40	2	10
163	1	50
190	3	10
205	3	10
250	5	N/A

5. Conclusions

In this work, the catalytic activities of untreated biochar and biochar ash have been demonstrated for the first time in the synthesis of glycerol carbonate and acetins from the reaction of glycerol, acetonitrile and CO_2.

Both the ash content and carbon content are shown to contribute to the overall activity of biochar. Biochar samples with higher ash contents were shown to be more active for the synthesis of glycerol carbonate and triacetin, compared to biochar samples with low or negligible ash contents. This was demonstrated by comparing the glycerol carbonate and triacetin yields from high ash samples (e.g., for RH 550, 0.0482 mol L^{-1} glycerol carbonate and 4.79×10^{-4} mol L^{-1} triacetin) with low ash samples (e.g., for SWP 550, negligible glycerol carbonate and negligible triacetin).

Potassium content was shown to influence the production of glycerol carbonate and triacetin. Biochars with higher surface potassium contents (e.g., OSR 550 with 17.1 at.% surface K) led to higher yields of product (0.0340 mol L^{-1} of glycerol carbonate, 7.16×10^{-4} mol L^{-1} triacetin) compared to biochars with lower surface potassium content (OSR 700 with 5.85 at.% surface K led to 1.25×10^{-3} mol L^{-1} glycerol carbonate and negligible triacetin). Biochar ash samples were also active in the production of glycerol carbonate and triacetin (e.g., for OSR 700-ash, 0.145 mol L^{-1} glycerol carbonate and 4.38×10^{-3} mol L^{-1} triacetin), despite much lower surface areas (BET surface areas between 19–38 m^2 g^{-1} for ash, compared to 51–390 m^2 g^{-1} for biochar). Removal of potassium content led to a decrease in glycerol carbonate production of at least 94% in all cases. Triacetin was no longer produced using ash samples after demineralisation.

Biochars with low or negligible ash content were shown to catalyse the formation of diacetin, indicating that the carbon content is also catalytically active. Graphitic carbon may be a positive influence in the formation of diacetin. Soft wood biochar led to higher quantities of diacetin than a commercial activated carbon (1.25×10^{-3} mol L^{-1} for SWP 550, 3.5×10^{-4} mol L^{-1} for AC). This was despite having a lower surface area (390 m^2 g^{-1} for SWP 550 compared to 729 m^2 g^{-1} for AC), and comparable elemental composition. Raman spectroscopy demonstrated that the carbon structure of soft wood biochar is more graphitic for SWP 550 than for AC (A_{D1}/A_G ratios of 1.32 and 2.82, respectively). Further work is required to clarify whether graphitic carbon is catalytically active in this reaction—for example, testing graphite for catalytic activity.

The ability of biochar ash to activate glycerol, as demonstrated herein, suggests that this may also be active for glycerol upgrading via other pathways, such as from glycerol and CO, or in other CO_2 utilisation reactions for producing organic carbonates. Future studies should consider how potassium and graphitic carbon are involved in these reaction mechanisms in order to apply the findings more generally to other reaction types.

More generally, it is recommended that future studies of catalytic activity in biochar consider a range of feedstock types, including low- and high-ash samples and conduct detailed mechanistic studies in order to develop robust structure–performance relationships. This will allow for an application-centred approach when developing a biochar for industrial or commercial applications, and hence improved process performance.

Supplementary Materials: The following are available online at http://www.mdpi.com/2073-4344/10/9/1067/s1. Figure S1: deconvolved Raman spectra for AC and SWB-550. Figures S2–S4: FTIR–ATR spectra for biochars, demineralised biochars and their ashes. Figures S5–S9: calibration curves for liquid phase products of glycerol carboxylation reaction. Table S1: settings used for obtaining Raman spectra. Table S2: Raman curve deconvolution peak assignments. Table S3: calibration sample concentrations. Table S4: product concentrations from three repeats of OSB-550, used to calculate the percentage error. Data for tables and figures are available online at 10.15131/shef.data.12783941.

Author Contributions: Conceptualization, C.C. and J.M.; methodology, C.C. and N.R.; software, C.C.; validation, J.M. and O.M.; formal analysis, C.C.; investigation, C.C.; resources, C.C, O.M. and J.M.; data curation, C.C.; writing—original draft preparation, C.C.; writing—review and editing, J.M.; visualization, C.C.; supervision, J.M.; project administration, J.M.; funding acquisition, C.C. and J.M. All authors have read and agreed to the published version of the manuscript.

Funding: This research was funded by the Engineering and Physical Sciences Research Council, via an EPSRC Doctoral Training Partnership award (C.C.); J.M. also acknowledges EPSRC support via grant EP/R026815/1.

Conflicts of Interest: The authors declare no conflict of interest. The funders had no role in the design of the study; in the collection, analyses or interpretation of data; in the writing of the manuscript, or in the decision to publish the results.

References

1. LMC. *Glycerine Report*; IHS, Oleoline; LMC: Oxford, UK, 2018.
2. Sonnati, M.O.; Amigoni, S.; Taffin de Givenchy, E.P.; Darmanin, T.; Choulet, O.; Guittard, F. Glycerol carbonate as a versatile building block for tomorrow: Synthesis, reactivity, properties and applications. *Green Chem.* **2013**, *15*, 283–306. [CrossRef]
3. Pagliaro, M.; Ciriminna, R.; Kimura, H.; Rossi, M.; Della Pina, C. From Glycerol to Value-Added Products. *Angew. Chem.* **2007**, *38*. [CrossRef]
4. Aresta, M.; Dibenedetto, A.; Fuji, Y.; Yamashita, H.; Koyano, K.; Tatsumi, K.T.; Schubert, G.; Fouassier, M.; Chupova, I.A.; Domen, K.; et al. Utilisation of CO_2 as a chemical feedstock: Opportunities and challenges. *Dalt. Trans.* **2007**, *98*, 2975. [CrossRef] [PubMed]
5. Li, H.; Gao, D.; Gao, P.; Wang, F.; Zhao, N.; Xiao, F.; Wei, W.; Sun, Y. The synthesis of glycerol carbonate from glycerol and CO_2 over $La_2O_2CO_3$–ZnO catalysts. *Catal. Sci. Technol.* **2013**, *3*, 2801. [CrossRef]
6. Li, H.; Jiao, X.; Li, L.; Zhao, N.; Xiao, F.; Wei, W.; Sun, Y.; Zhang, B. Synthesis of glycerol carbonate by direct carbonylation of glycerol with CO_2 over solid catalysts derived from Zn/Al/La and Zn/Al/La/M (M = Li, Mg and Zr) hydrotalcites. *Catal. Sci. Technol.* **2015**, *5*, 989–1005. [CrossRef]
7. Razali, N. The Synthesis of Glycerol Carbonate from Glycerol and Carbon Dioxide over Heterogeneous Catalysts. Ph.D. Thesis, University of Sheffield, Sheffield, UK, 2017.
8. Kong, P.S.; Aroua, M.K.; Daud, W.M.A.W.; Lee, H.V.; Cognet, P.; Pérès, Y. Catalytic role of solid acid catalysts in glycerol acetylation for the production of bio-additives: A review. *RSC Adv.* **2016**, *6*, 68885–68905. [CrossRef]
9. Sandesh, S.; Manjunathan, P.; Halgeri, A.B.; Shanbhag, G.V. Glycerol acetins: Fuel additive synthesis by acetylation and esterification of glycerol using cesium phosphotungstate catalyst. *RSC Adv.* **2015**, *5*, 104354–104362. [CrossRef]
10. Konwar, L.J.; Mäki-Arvela, P.; Begum, P.; Kumar, N.; Thakur, A.J.; Mikkola, J.-P.; Deka, R.C.; Deka, D. Shape selectivity and acidity effects in glycerol acetylation with acetic anhydride: Selective synthesis of triacetin over Y-zeolite and sulfonated mesoporous carbons. *J. Catal.* **2015**, *329*, 237–247. [CrossRef]
11. Algoufi, Y.T.; Hameed, B.H. Synthesis of glycerol carbonate by transesterification of glycerol with dimethyl carbonate over K-zeolite derived from coal fly ash. *Fuel Process. Technol.* **2014**, *126*, 5–11. [CrossRef]
12. Ozorio, L.P.; Pianzolli, R.; da Cruz Machado, L.; Miranda, J.L.; Turci, C.C.; Guerra, A.C.O.; Souza-Aguiar, E.F.; Mota, C.J.A. Metal-impregnated zeolite Y as efficient catalyst for the direct carbonation of glycerol with CO_2. *Appl. Catal. A Gen.* **2015**, *504*, 187–191. [CrossRef]
13. Razali, N.A.; Conte, M.; McGregor, J. The role of impurities in the La_2O_3 catalysed carboxylation of crude glycerol. *Catal. Lett.* **2019**, *149*, 1403–1414. [CrossRef]
14. Indran, V.P.; Syuhada Zuhaimi, N.A.; Deraman, M.A.; Maniam, G.P.; Yusoff, M.M.; Yun Hin, T.-Y.; Ab Rahim, M.H. An accelerated route of glycerol carbonate formation from glycerol using waste boiler ash as catalyst. *RSC Adv.* **2014**, *4*, 25257–25267. [CrossRef]
15. Ahmad, M.; Rajapaksha, A.U.; Lim, J.E.; Zhang, M.; Bolan, N.; Mohan, D.; Vithanage, M.; Lee, S.S.; Ok, Y.S. Biochar as a sorbent for contaminant management in soil and water: A review. *Chemosphere* **2014**, *99*. [CrossRef] [PubMed]
16. Hernandez-Mena, L.E.; Pecora, A.B.; Beraldo, A.L. Slow pyrolysis of bamboo biomass: Analysis of biochar properties. *Chem. Eng. Trans.* **2014**, *37*, 115–120. [CrossRef]
17. Klinghoffer, N.B.; Castaldi, M.J.; Nzihou, A. Influence of char composition and inorganics on catalytic activity of char from biomass gasification. *Fuel* **2015**, *157*, 37–47. [CrossRef]
18. Davies, G.; El Sheikh, A.; Collett, C.; Yakub, I.; McGregor, J. Catalytic Carbon Materials from Biomass. In *Emerging Carbon Materials for Catalysis*; Sadjadi, S., Ed.; Elsevier: Amsterdam, The Netherlands, 2020.
19. Abdullah, S.H.Y.S.; Hanapi, N.H.M.; Azid, A.; Umar, R.; Juahir, H.; Khatoon, H.; Endut, A. A review of biomass-derived heterogeneous catalyst for a sustainable biodiesel production. *Renew. Sustain. Energy Rev.* **2017**, *70*, 1040–1051. [CrossRef]
20. Lee, J.; Kim, K.H.; Kwon, E.E. Biochar as a Catalyst. *Renew. Sustain. Energy Rev.* **2017**, *77*, 70–79. [CrossRef]
21. Cao, X.; Sun, S.; Sun, R. Application of biochar-based catalysts in biomass upgrading: A review. *RSC Adv.* **2017**, *7*, 48793–48805. [CrossRef]

22. Wang, L.; Ok, Y.S.; Tsang, D.C.W.; Alessi, D.S.; Rinklebe, J.; Wang, H.; Mašek, O.; Hou, R.; O'Connor, D.; Hou, D. New trends in biochar pyrolysis and modification strategies: Feedstock, pyrolysis conditions, sustainability concerns and implications for soil amendment. *Soil Use Manag.* **2020**, *36*, 358–386. [CrossRef]
23. Zhao, L.; Cao, X.; Masek, O.; Zimmerman, A. Heterogeneity of biochar properties as a function of feedstock and production temperatures. *J. Hazard. Mater.* **2013**, *256–257*, 1–9. [CrossRef]
24. Manyà, J.J. Pyrolysis for Biochar Purposes: A Review to Establish Current Knowledge Gaps and Research Needs. *Environ. Sci. Technol.* **2012**, *46*, 7939–7954. [CrossRef]
25. Jindo, K.; Mizumoto, H.; Sawada, Y.; Sanchez-Monedero, M.A.; Sonoki, T. Physical and chemical characterization of biochars derived from different agricultural residues. *Biogeosciences* **2014**, *11*, 6613–6621. [CrossRef]
26. Titirici, M.-M.; White, R.J.; Brun, N.; Budarin, V.L.; Su, D.S.; del Monte, F.; Clark, J.H.; MacLachlan, M.J. Sustainable carbon materials. *Chem. Soc. Rev.* **2015**, *44*, 250–290. [CrossRef]
27. Zhao, Y.; Feng, D.; Zhang, Y.; Huang, Y.; Sun, S. Effect of pyrolysis temperature on char structure and chemical speciation of alkali and alkaline earth metallic species in biochar. *Fuel Process. Technol.* **2016**, *141*, 54–60. [CrossRef]
28. Asadullah, M.; Zhang, S.; Min, Z.; Yimsiri, P.; Li, C.-Z. Effects of biomass char structure on its gasification reactivity. *Bioresour. Technol.* **2010**, *101*, 7935–7943. [CrossRef]
29. Bachmann, H.J.; Bucheli, T.D.; Dieguez-Alonso, A.; Fabbri, D.; Knicker, H.; Schmidt, H.-P.; Ulbricht, A.; Becker, R.; Buscaroli, A.; Buerge, D.; et al. Toward the Standardization of Biochar Analysis: The COST Action TD1107 Interlaboratory Comparison. *J. Agric. Food Chem.* **2016**, *64*, 513–527. [CrossRef]
30. Crombie, K.; Mašek, O.; Cross, A.; Sohi, S. Biochar-synergies and trade-offs between soil enhancing properties and C sequestration potential. *GCB Bioenergy* **2015**, *7*, 1161–1175. [CrossRef]
31. Brewer, C.E.; Unger, R.; Schmidt-Rohr, K.; Brown, R.C. Criteria to Select Biochars for Field Studies based on Biochar Chemical Properties. *Bioenergy Res.* **2011**, *4*, 312–323. [CrossRef]
32. Abu El-Rub, Z.; Bramer, E.A.; Brem, G. Experimental comparison of biomass chars with other catalysts for tar reduction. *Fuel* **2008**, *87*, 2243–2252. [CrossRef]
33. Dehkhoda, A.M.; West, A.H.; Ellis, N. Biochar based solid acid catalyst for biodiesel production. *Appl. Catal. A Gen.* **2010**, *382*, 197–204. [CrossRef]
34. Kastner, J.R.; Miller, J.; Geller, D.P.; Locklin, J.; Keith, L.H.; Johnson, T. Catalytic esterification of fatty acids using solid acid catalysts generated from biochar and activated carbon. *Catal. Today* **2012**, *190*, 122–132. [CrossRef]
35. Moussavi, G.; Khosravi, R. Preparation and characterization of a biochar from pistachio hull biomass and its catalytic potential for ozonation of water recalcitrant contaminants. *Bioresour. Technol.* **2012**, *119*, 66–71. [CrossRef] [PubMed]
36. Ormsby, R.; Kastner, J.R.; Miller, J. Hemicellulose hydrolysis using solid acid catalysts generated from biochar. *Catal. Today* **2012**, *190*, 89–97. [CrossRef]
37. Rafi, J.M.; Rajashekar, A.; Srinivas, M.; Rao, B.V.S.K.; Prasad, R.B.N.; Lingaiah, N. Esterification of glycerol over a solid acid biochar catalyst derived from waste biomass. *RSC Adv.* **2015**, *5*, 44550–44556. [CrossRef]
38. Shen, Y.; Zhao, P.; Shao, Q.; Ma, D.; Takahashi, F.; Yoshikawa, K. In-situ catalytic conversion of tar using rice husk char-supported nickel-iron catalysts for biomass pyrolysis/gasification. *Appl. Catal. B Environ.* **2014**, *152*, 140–151. [CrossRef]
39. Wang, F.J.; Zhang, S.; Chen, Z.D.; Liu, C.; Wang, Y.G. Tar reforming using char as catalyst during pyrolysis and gasification of Shengli brown coal. *J. Anal. Appl. Pyrolysis* **2014**, *105*. [CrossRef]
40. Yu, J.T.; Dehkhoda, A.M.; Ellis, N. Development of Biochar-based Catalyst for Transesterification of Canola Oil. *Energy Fuels* **2011**, *25*, 337–344. [CrossRef]
41. Shen, B.; Chen, J.; Yue, S.; Li, G. A comparative study of modified cotton biochar and activated carbon based catalysts in low temperature SCR. *Fuel* **2015**, *156*, 47–53. [CrossRef]
42. Bazargan, A.; Kostić, M.D.; Stamenković, O.S.; Veljković, V.B.; McKay, G. A calcium oxide-based catalyst derived from palm kernel shell gasification residues for biodiesel production. *Fuel* **2015**, *150*, 519–525. [CrossRef]
43. Chakraborty, R.; Bepari, S.; Banerjee, A. Transesterification of soybean oil catalyzed by fly ash and egg shell derived solid catalysts. *Chem. Eng. J.* **2010**, *165*, 798–805. [CrossRef]

44. Ofori-Boateng, C.; Lee, K.T. The potential of using cocoa pod husks as green solid base catalysts for the transesterification of soybean oil into biodiesel: Effects of biodiesel on engine performance. *Chem. Eng. J.* **2013**, *220*, 395–401. [CrossRef]
45. Riadi, L.; Purwanto, E.; Kurniawan, H.; Oktaviana, R. Effect of Bio-based Catalyst in Biodiesel Synthesis. *Procedia Chem.* **2014**, *9*, 172–181. [CrossRef]
46. Feng, D.; Zhang, Y.; Zhao, Y.; Sun, S.; Gao, J. Improvement and maintenance of biochar catalytic activity for in-situ biomass tar reforming during pyrolysis and H_2O/CO_2 gasification. *Fuel Process. Technol.* **2018**, *172*, 106–114. [CrossRef]
47. Lisowski, P.; Colmenares, J.C.; Mašek, O.; Lisowski, W.; Lisovytskiy, D.; Kamińska, A.; Łomot, D. Dual Functionality of TiO_2/Biochar Hybrid Materials: Photocatalytic Phenol Degradation in the Liquid Phase and Selective Oxidation of Methanol in the Gas Phase. *ACS Sustain. Chem. Eng.* **2017**, *5*, 6274–6287. [CrossRef]
48. Indran, V.P.; Haji Saud, A.S.; Maniam, G.P.; Yusoff, M.M.; Taufiq-Yap, Y.H.; Rahim, M.H.A.; Alloin, F. Versatile boiler ash containing potassium silicate for the synthesis of organic carbonates. *RSC Adv.* **2016**, *6*, 34877–34884. [CrossRef]
49. Paroo Indran, V.; Sajidah Haji Saud, A.; Pragas Maniam, G.; Hin Taufiq-Yap, Y.; Hasbi Ab Rahim, M. Viable Glycerol Carbonate Synthesis Through Direct Crude Glycerol Utilization from Biodiesel Industry. *Waste Biomass Valorization* **2017**. [CrossRef]
50. Nosyrev, I.E.; Gruber, R.; Cagniant, D.; Krzton, A.; Pajak, J.; Stefanova, M.D.; Grishchuk, S. DRIFT spectroscopic characterization of coal samples modified by chemical treatments. *Fuel* **1996**, *75*, 1549–1556. [CrossRef]
51. Huo, C.-F.; Wu, B.-S.; Gao, P.; Yang, Y.; Li, Y.-W.; Jiao, H. The Mechanism of Potassium Promoter: Enhancing the Stability of Active Surfaces. *Angew. Chem. Int. Ed.* **2011**, *50*, 7403–7406. [CrossRef]
52. Rokicki, G.; Rakoczy, P.; Parzuchowski, P.; Sobiecki, M. Hyperbranched aliphatic polyethers obtained from environmentally benign monomer: Glycerol carbonate. *Green Chem.* **2005**, *7*, 529–539. [CrossRef]
53. Gómez-Jiménez-Aberasturi, O.; Ochoa-Gómez, J.R.; Pesquera-Rodríguez, A.; Ramírez-López, C.; Alonso-Vicario, A.; Torrecilla-Soria, J. Solvent-free synthesis of glycerol carbonate and glycidol from 3-chloro-1,2-propanediol and potassium (hydrogen) carbonate. *J. Chem. Technol. Biotechnol.* **2010**, *85*, 1663–1670. [CrossRef]
54. Mašek, O.; Buss, W.; Brownsort, P.; Rovere, M.; Tagliaferro, A.; Zhao, L.; Cao, X.; Xu, G. Potassium doping increases biochar carbon sequestration potential by 45%, facilitating decoupling of carbon sequestration from soil improvement. *Sci. Rep.* **2019**, *9*, 1–8. [CrossRef] [PubMed]
55. Buss, W.; Bogush, A.; Ignatyev, K.; Masek, O. Unlocking the fertiliser potential of waste-derived biochar. *ACS Sustain. Chem. Eng.* **2020**. [CrossRef]
56. Collett, C.H.; McGregor, J. Things go better with coke: The beneficial role of carbonaceous deposits in heterogeneous catalysis. *Catal. Sci. Technol.* **2016**, *6*, 363–378. [CrossRef]
57. UK Biochar Research Centre. Standard Biochars. Available online: https://www.biochar.ac.uk/standard_materials.php (accessed on 17 May 2017).
58. Mašek, O.; Buss, W.; Roy-Poirier, A.; Lowe, W.; Peters, C.; Brownsort, P.; Mignard, D.; Pritchard, C.; Sohi, S. Consistency of biochar properties over time and production scales: A characterisation of standard materials. *J. Anal. Appl. Pyrolysis* **2018**, *132*, 200–210. [CrossRef]
59. Moreno-Castilla, C.; Carrasco-Marín, F.; Maldonado-Hódar, F.J.; Rivera-Utrilla, J. Effects of non-oxidant and oxidant acid treatments on the surface properties of an activated carbon with very low ash content. *Carbon* **1997**, *36*, 145–151. [CrossRef]
60. Nowakowski, D.J.; Jones, J.M. Uncatalysed and potassium-catalysed pyrolysis of the cell-wall constituents of biomass and their model compounds. *J. Anal. Appl. Pyrolysis* **2008**, *83*, 12–25. [CrossRef]
61. Morgan, M.E.; Jenkins, R.G.; Walker, P.L., Jr. Inorganic constituents in American lignites. *Fuel* **1981**, *60*, 189–193. [CrossRef]
62. Raveendran, K.; Ganesh, A.; Khilar, K.C. Influence of mineral matter on biomass pyrolysis characteristics. *Fuel* **1995**, *74*, 1812–1822. [CrossRef]
63. Specac. *The Specac Quest: How the ATR Accessory Works*; Specac: Orpington, UK, 2016.
64. ASTM. *International Standard Test Methods for Proximate Analysis of Coal and Coke by Macro Thermogravimetric Analysis*; ASTM: West Conshohocken, PA, USA, 2010.

65. National Physical Laboratory. Calibration Software and Reference Materials for Electron Spectrometers. Available online: http://www.npl.co.uk/science-technology/surface-and-nanoanalysis/services/calibration-software-and-reference-materials-for-electron-spectrometers (accessed on 8 August 2018).
66. Harkins, W.D.; Jura, G. The Decrease (π) of Free Surface Energy (γ) as a Basis for the Development of Equations for Adsorption Isotherms; and the Existence of Two Condensed Phases in Films on Solids. *J. Chem. Phys.* **1944**, *12*, 112–113. [CrossRef]
67. Horváth, G.; Kawazoe, K. Method for the calculation of effective pore size distribution in molecular sieve carbon. *J. Chem. Eng. Jpn.* **1983**, *16*, 470–475. [CrossRef]
68. Ayala, P.; Maia da Costa, M.E.H.; Prioli, R.; Freire, F.L. Nano- and micro-scale wear of fluorinated carbon films. *Surf. Coat. Technol.* **2004**, *182*, 335–341. [CrossRef]
69. Tarrant, R.N.; McKenzie, D.R.; Bilek, M.M.M. Raman characterisation of PIII multilayer carbon films. *Diam. Relat. Mater.* **2004**, *13*, 1422–1426. [CrossRef]
70. Li, X.; Hayashi, J.; Li, C. Volatilisation and catalytic effects of alkali and alkaline earth metallic species during the pyrolysis and gasification of Victorian brown coal. Part VII. Raman spectroscopic study on the changes in char structure during the catalytic gasification in air. *Fuel* **2006**, *85*, 1509–1517. [CrossRef]
71. Chia, C.H.; Gong, B.; Joseph, S.D.; Marjo, C.E.; Munroe, P.; Rich, A.M. Imaging of mineral-enriched biochar by FTIR, Raman and SEM–EDX. *Vib. Spectrosc.* **2012**, *62*, 248–257. [CrossRef]

© 2020 by the authors. Licensee MDPI, Basel, Switzerland. This article is an open access article distributed under the terms and conditions of the Creative Commons Attribution (CC BY) license (http://creativecommons.org/licenses/by/4.0/).